



Formic acid-to-hydrogen on Pd/AC catalysts: Kinetic study with catalytic deactivation

Celia Martin, Asunción Quintanilla^{*}, Gonzalo Vega, Jose A. Casas

Department of Chemical Engineering, Universidad Autónoma de Madrid, Spain

ARTICLE INFO

Keywords:

Hydrogen storage
LOHC
Formic acid
Catalyst deactivation
Kinetic model

ABSTRACT

A kinetic model for formic acid (FA) decomposition over a commercial 10 wt% Pd/AC catalyst has been developed to describe the hydrogen production and to understand the deactivation mechanism. The kinetic data were obtained in a batch slurry reactor in absence of mass transfer limitation at: $C_{FA,0} = 0.25\text{--}2\text{ M}$, $C_{CAT} = 1\text{ g L}^{-1}$, $T = 25\text{--}85\text{ °C}$ and $P = 1\text{ atm}$. The catalyst stability was studied in successive cycles at different temperatures. Fresh, used and regenerated Pd/AC catalysts were deeply characterized to gain insight into the activity, selectivity and stability. H_2 and CO_2 were the only reaction products detected. The reaction follows a first order kinetic for FA while the activity shows exponential decay with the initial FA concentration and reaction temperature. This paper represents a step forward in the on-site hydrogen production technology by using FA as liquid organic hydrogen carrier.

1. Introduction

Hydrogen is a versatile clean, and safe energy carrier that, complementary to green electricity, can help to tackle the decarbonization challenge of the energy sector to limit the effects of climate change [1]. Hydrogen has the highest energy per unit mass of any fuel ($120\text{ MJ kg}^{-1} H_2$ vs. 44 MJ kg^{-1} gasoline); however, its low density results in low energy per unit volume (only 8 MJ L^{-1} whereas gasoline is 32 MJ L^{-1}), therefore requiring the development of advanced storage methods that have potential for higher energy density, particularly interesting for onboard fuel cells vehicles [2,3]. Hydrogen can be stored using material-based approaches namely, adsorbents (such as metallic organic frameworks as $Zn_4O(BDC)_3$ and $Mn_3[(Mn_4Cl)_3(BTT)_8]_2$) [4], metal hydrides (such as alanates, especially $NaAlH_4$) [5], and complex hydrides (as perovskite-type borohydride, $NH_4Ca(BH_4)_3$) [6] and liquid-phase chemical hydrogen storage (particularly metal-boron hydrides, ammonia borane, hydrazine hydrate, formic acid and aromatic compounds) [3,7,9]. All these materials have demonstrated the potential to be used as hydrogen sources but each of them has its own merits and drawbacks. In general, the solid-state hydrogen storage materials require high temperatures to desorb hydrogen molecules, they provide a slow hydrogen release rate and are deteriorated with successive cycling [7,10]. The liquid-phase hydrogen storage material is a safer alternative to the physical hydrogen storage, they have a higher reversibility and

higher storage capacities [8,11]. Furthermore, in case of liquid organic chemicals, commonly known as LOHCs (Liquid Organic Hydrogen Carriers), the hydrogen storage and transportation are a low investment risk due to the high compatibility with the current transport infrastructure for hydrocarbons fuels [12]. Since 1980, it has been an intense research work demonstrating that hydrogen can be chemically stored and extracted on demand from an organic carrier based on reversible catalytic hydrogenation-dehydrogenation reactions [13,14]. The main research efforts have been devoted to the development of selective and stable catalysts to efficiently conduct the chemical process at a mild operation temperature [15,16]. The typical systems are benzene/cyclohexane, toluene/methylcyclohexane and naphthalene/decalin, with a storage capacity of 7.1 wt% (cyclohexane), 6.1 wt% (methylcyclohexane) and 7.2 wt% (decalin), respectively. These catalytic systems require temperatures above 300 °C to achieve full conversions in presence of a potassium-promoted 5 wt%Pt/ $\gamma\text{-Al}_2\text{O}_3$ [14]. Most recently, carbazoles and substituted carbazoles are intended as further organic materials (5.7–6.2 wt% of hydrogen storage capacity) to enable the hydrogen delivering at temperatures of about 200 °C . These strict reaction conditions unable their application for onboard fuel cells vehicles and they are rather considered as storage and transport medium in filling stations for fuel-cell-powered cars [14]. As an alternative for portable applications, formic acid (FA) has been suggested and studied as a promising LOHC owing to its appropriate characteristics: liquid

^{*} Corresponding author.

E-mail address: asun.quintanilla@uam.es (A. Quintanilla).

<https://doi.org/10.1016/j.apcatb.2022.121802>

Received 1 May 2022; Received in revised form 22 July 2022; Accepted 27 July 2022

Available online 28 July 2022

0926-3373/© 2022 The Author(s). Published by Elsevier B.V. This is an open access article under the CC BY license (<http://creativecommons.org/licenses/by/4.0/>).

state at ambient temperature, highly stable, nontoxic and environmental benign, and relatively high hydrogen storage capacity (4.4 wt%) [17, 19]. The CO₂ can be hydrogenated to FA to have a CO₂ neutral process or, most interesting, FA can derive from a biomass feedstock [17,18,20, 21].

The FA is decomposed via catalytic dehydrogenation reaction to produce H₂ and CO₂ but also, FA can be dehydrated, which generates CO and H₂O. This last reaction must be avoided as CO deactivates the fuel cell catalysts. For that, the reaction temperature of the FA decomposition reaction must be controlled ($T < 60\text{ }^{\circ}\text{C}$) [22] and the appropriate catalyst used [23]. Thus, the design of effective catalysts has been intensively investigated to produce CO-free H₂ from FA decomposition at ambient temperature. Several reviews analyze the advances in the synthesis of homogeneous and heterogeneous catalysts for FA decomposition [18,19,23,24]. The most efficient solid catalyst is Pd nanoparticles immobilized on carbon-based supports [25]. The most active and selective one is Pd on activated carbon, Pd/AC, with a Pd loading from 5 to 10 wt% [9,23].

Regarding to the features of the Pd/AC for the liquid-phase FA decomposition reaction, the Pd particle sizes (from 2 to 5 nm) and the surface electronic states of the Pd (this is, an adequate Pd^{δ+}/Pd⁰ ratio) are the most critical factors determining the performance of the catalyst aiming at the compromise between high catalytic activity and adequate recyclability [9,25,29]. Besides, the presence of Pd-PdO interfaces increases the catalyst activity and, also, the selectivity towards the dehydrogenation reaction, overcoming by this way, the CO poisoning [30]. Despite these considerations, the progressive deactivation of Pd catalyst upon reaction is unavoidable due to several reasons such as the occupation of the Pd active sites by protons, CO₂, H₂O or formate anion (HCOO⁻) [9,22,31], FA fouling [31], agglomeration of the Pd particle sizes [9] and, in a few works, by CO poisoning [9,32,33]. The preparation of expensive bimetallic and trimetallic Pd catalyst (*viz.* AuPd, AgPd, NiPd, CuPd, Pd-MnO_x, NiAuPd, CoAgPd, PtRuBi, PdCuCr and AgPd-MnO_x) with alloyed structure and small particle size (2–5 nm) improves the stability in the catalyst recycling [18,19,28]. Also, the use of low reaction temperatures, typically from 25 to 60 °C, improves the stability of the Pd/AC catalyst [22]. In this case, to compensate for the lower reaction rates, particularly at ambient reaction temperatures, sodium formate (SF) is added as promoter to favor the FA deprotonation, the rate determining step in the reaction pathway [19,34].

Despite the evident interest for the use of FA as hydrogen storage (more than 1250 papers published in the last decade, source: Isi Web of Knowledge), it has not been found a kinetic study to model the FA decomposition reaction in liquid phase that helps to the reaction engineering for the onsite hydrogen production. Previous works report apparent activation energy values from 30 to 65 kJ mol⁻¹ for monometallic Pd nanoparticles on carbon-based supports [9,22,26,29,35,39] (see Table S1 of the Supporting Information) and some of them, apparent reaction orders lower than 1 [9,22] at very short reaction times but a comprehensive kinetic study considering the fast deactivation of the Pd/AC has not been considered so far.

The motivation of the present work is to contribute to the development of hydrogen storage and transportation technology using FA as sustainable hydrogen carrier. The aim is to provide an accurate kinetic model for FA dehydrogenation reaction over a commercial Pd/AC catalyst that enables the further reaction engineering for the optimization of the chemical reactor, feed composition and operating conditions. The mathematical model will combine the kinetic reaction in absence of mass transfer limitation and the catalyst deactivation to describe the temporal evolution of FA concentration as a function of the reaction temperature and initial FA concentration used.

2. Experimental

2.1. Pd/AC catalyst and characterization

A commercial Pd (10 wt%) supported on activated carbon catalyst (10 wt%Pd/AC, henceforth Pd/AC) was supplied by Evonik (Noblyst® P1070) in powder form. The catalyst was dried overnight at 60 °C before use to remove the content of water.

Different techniques were used to characterize the fresh and used Pd/AC catalysts. The average Pd particle size was examined by the transmission electron microscopy operating at 200 kV (TEM, JEOL 2100 F). The Pd dispersion was obtained by CO chemisorption at room temperature (3Flex, Micromeritics). Typically, the sample was reduced in hydrogen for 1 h and flushed with helium for 0.5 h. Then, CO was introduced as pulses and the response was recorded using a TCD detector. It is assumed that the stoichiometric ratio of adsorbed CO and Pd surface atoms is one. X-ray diffraction (XRD) patterns were recorded using a Bruker D5000 (Siemens) X-ray diffractometer with Cu Kα radiation ($\lambda = 0.154178\text{ nm}$) operating at 40 kV and 30 mA. 2θ was scanning from 10° up to 80° with a step size of 0.0486°. The exposed Pd surface species (Pd⁰, Pd^{δ+}) were quantified by X-ray photoelectron spectroscopy (XPS). The spectra measurements were performed with the PHI5000 VersaProbe II using a monochromatic Al-Kα X-ray beam (1486.6 eV). Charge referencing was measured against adventitious carbon (C 1 s at 284.8 eV). The specific surface area (S_{BET}) and externa area (A_{ext}) were measured at 77 K using a Micromeritics Tristar 3000 apparatus nitrogen using the Brunauer-Emmett-Teller (BET) method. Before the measurement, the samples were outgassed at 120 °C overnight. The elemental composition of the catalysts was measured using a LECO CHNS-932 analyzer. The overall Pd loading in the catalysts after reaction was measured by total reflection X-ray fluorescence (TXRF) using a benchtop S2 PICOFOX TXRF spectrometer (Bruker Nano). Besides, the thermogravimetric-differential thermal analysis (TGA-DTA) was performed in a TA Instruments Discovery STD 650, equipped with an online ThermoStar GSD 301 T3 Benchtop mass spectrometer (MS) under an helium flow 90 mL min⁻¹ and the following temperature program: 15 min isothermal, heating to 40 °C with a ramp of 2 °C min⁻¹, 60 min isothermal and then heating to 220 °C with a ramp of 10 °C min⁻¹. Attenuated total reflection (ATR) spectroscopy was performed to detect CO and CO₂ adsorbed on Pd nanoparticles. A Bruker vector 22 FTIR spectrometer equipped with a MCT detector and Harrick diffuse reflectance accessory was used. Spectra was obtained with apparatus loading on ~ 0.2 g of sample mixed with KBr scanning at 4 cm⁻¹ resolution with 20 scans from 4000 to 450 cm⁻¹.

2.2. Catalytic dehydrogenation of formic acid

The experiments were conducted in a stirred slurry reactor operated in semi-batch mode. A 100 mL three-necked glass reactor magnetically stirrer was submerged in a silicon hot bath at a pre-set temperature under an ambient atmosphere. It was equipped with a thermometer, a syringe for the injection of the formic acid reactant and a gas outlet tube connected to a buret filled with water to measure the volume of the gas release upon reaction. In a typical experiment, 60 mL of mili-Q water (Wasserlab) with the desired amount of catalyst was placed into the reactor and vigorously stirred. Once the reaction temperature was achieved, 10 mL of aqueous formic acid solution at the selected concentration is injected being this the starting time for the reaction. The evolve gas volume is monitored by recording the water displacement in the buret with reaction time. Some selected reactions were repeated several times to analyze the chemical composition of the gas with the reaction time. The following operating conditions were used to carry out the kinetic study: stirring speed (ω) = 200–900 rpm, catalyst concentration (C_{CAT}) = 0.5–2 g L⁻¹, initial formic acid concentration ($C_{\text{FA},0}$) = 0.25–2 M and reaction temperature (T) = 25–85 °C. In some experiments, SF as additive was used to promote the FA dehydrogenation

reaction rate (SF:FA = 0.8:1 molar ratio). For reusability, the catalyst was recovered from the reactor effluent by filtration and dried overnight at 60 °C. Additionally, the regeneration of the used catalyst was carried out by heating the dried catalyst at 150 °C during 12 h in air atmosphere.

An additional experiment was carried out by pretreating the commercial catalyst with CO₂ according to the following procedure: 0.07 g of 10 wt%Pd/AC catalyst was charged to the reactor and flush with helium (2 mL min⁻¹, overnight) and after with CO₂ at room temperature (2 mL min⁻¹, overnight). The treated catalyst was used in reaction at the following standard operating conditions: C_{FA,0} = 1 M, C_{CAT} = 1 g L⁻¹, ω = 650 rpm and P = 1 atm. The surface acidity of the “as-received” and CO₂ pre-treated Pd/CA catalysts was measured by the pH of their aqueous suspension (0.005 g of catalyst stirred with 2 mL of distilled water for 3 days).

From the volume of the evolved gas (V_{gas}) vs. reaction time obtained in each run, the FA concentration (C_{FA}), FA conversion (X_{FA}) and initial TOF values (TOF₀), the last one defined as the mol of formic acid converted per mol of Pd active site and time, were calculated as the following equations:

$$C_{FA} \left(\frac{\text{mol}}{\text{L}} \right) = \frac{n_{H_2}}{V_L} \text{ when } n_{H_2} \text{ (mol)} = \frac{P \cdot V_{\text{gas}}}{2RT} \bullet 100 \quad (1)$$

$$X_{FA} (\%) = \frac{C_{FA,0} - C_{FA}}{C_{FA,0}} \bullet 100 \quad (2)$$

$$TOF_0 (h^{-1}) = \frac{(-r_{FA})_{w,0} \cdot \text{at.wt. Pd}}{\%wtPd \cdot D \cdot 60 \left(\frac{\text{min}}{h} \right)} \quad (3)$$

Here, $(-r_{FA})_{w,0}$ is the initial FA decomposition rate in mol_{FA} g_{CAT}⁻¹ min⁻¹. It is calculated as the slope of the temporal FA concentration profile to convert 2% of FA (X_{FA} = 2%). Besides, at.wt. is the Pd atomic weight (106.4 g mol⁻¹); %wt is the Pd weight percentage on the activated carbon, 10 wt%; and D is the Pd dispersion measured by CO chemisorption.

2.3. Analytical methods

The composition of the evolve gas was analyzed by a gas chromatograph (Agilent 6890) equipped with a thermal conductivity detector using a Varian select permanent gases/CO₂ column. The H₂, CO, CO₂, O₂ and N₂ gases were calibrated using two commercial standards. He was used as carrier gas. The FA concentration in the fixed-bed reactor effluent was monitored by using ionic chromatography (IC) equipped with a conductivity detector (Metrohm 883 IC) using a Metrosep A supp 5 column (250 × 4 mm) as stationary phase and 0.7 mL min⁻¹ of an aqueous solution of 3.2 mM Na₂CO₃ and 1 mM NaHCO₃ as the mobile phase. Pd concentration in the liquid phase was measured by TXRF.

2.4. Kinetic model

The mass balance of FA in the isothermal stirred batch reactor can be expressed as:

$$(-r_{FA})_w \left(\frac{\text{mol}_{FA}}{\text{g}_{CAT} \cdot \text{min}} \right) = -\frac{dC_{FA}}{C_{CAT} \bullet dt} \quad (4)$$

The FA reaction rate depends not only on the concentration of formic acid and temperature, but also on the activity of the catalyst (a), as shown in the following equation:

$$(-r_{FA})_w = (-r_{FA})_{w,t=0} \bullet a \quad (5)$$

The kinetic equations proposed for $(-r_{FA})_{w,t=0}$, the reaction rate of the fresh catalyst in absence of deactivation, to describe the influence of temperature and concentration are potential equations, Langmuir-Hinshelwood-Hougen-Watson (LHHW) and Eley-Rideal (ER) kinetics. On the other hand, the activity decay always attends to a power law equation:

$$-\frac{da}{dt} (\text{min}^{-1}) = k_d \bullet a^m \quad (6)$$

where k_d is the deactivation kinetic constant (in min⁻¹) and m is the empirical exponent, which takes values of 0, 1 and 2 for linear, exponential, or hyperbolic decay curves, respectively.

OriginLab 2017 program was used for the non-linear regressions aimed at calculating the kinetic parameters. It is based on the Levenberg-Marquardt algorithm to minimize the chi-square (χ²) function, defined as the residual sum of squares (RSS) by the degrees of freedom. The initial conditions considered are: C_{FA} = C_{FA,0} at t = 0 min. The model discrimination was based on statistical analysis, considering the coefficient of determination (R²) closer to one, and the physical meaning of the estimated parameters.

3. Results and discussion

3.1. Catalyst characterization of fresh Pd/AC

Fig. 1a-b display the typical TEM image and particle size distribution for the fresh Pd/AC catalyst, respectively. The average particle size is 1.6 ± 0.2 nm. By CO chemisorption, the measured Pd dispersion was 23.8%. The XRD pattern, Fig. 1c, shows the characteristic peaks of activated carbon (2θ = 24.7°, 57.3° and 61.8°), PdO (2θ = 33.8° and 43.8°) and metallic Pd (2θ = 40.4°, 46.8°, 68.3° and 82.1°) [9,34]. Note the presence of crystalline PdO phase, with a higher amount of under-coordinated PdO surface such as PdO(101) than PdO(110) surface, both desirable species for a high catalyst efficiency and selectivity [30]. The presence of Pd²⁺ species was also confirmed by XPS. Fig. 1d shows the XPS spectra in the Pd 3d region. Each Pd species displays two peaks due to the 3d_{5/2} and 3d_{3/2} transitions. Peaks at 335.5 and 340.9 eV are ascribed to Pd⁰ while peaks at 337.5 and 342.6 eV to Pd²⁺, with PdO being the most likely species [9,27,29,37]. The ratio Pd²⁺/Pd⁰ is approximately 2.4.

The BET surface area (S_{BET}) and the external area (A_{ext}) measured were 887 and 404 m² g⁻¹, respectively, with pore volume of 0.3 cc g⁻¹ and pore size of 1.4 nm, which in accordance with the IUPAC classification, Pd/AC is a microporous material.

3.2. Influence of the operating conditions on the H₂ production

The kinetic control was verified prior to the analysis of the operating conditions. The appropriate stirring velocity (ω = 650 rpm) and mass of catalyst (W_{CAT} = 0.07 g) were chosen to avoid external transport rate limitations. The results, demonstrating the adequacy the selection attending to the influence of both variables, ω and W_{CAT}, on the initial FA reaction rates are provided in Fig. S1 of the Supporting Information. Besides, the catalyst was used in powder form, d_{particle} = 25 μm, to avoid internal mass transfer control (see the calculations in the Supporting Information, after Fig. S1).

3.2.1. Effect of the reaction temperature

Fig. 2 depicts the results obtained in a wide range of temperature, from 25 to 85 °C. As expected by the related works in the literature using a batch reactor [9,22,29,34-39] the volume of evolved gas increases with the course of the reaction and tends to reach an asymptotic value (Fig. 2a). At high temperatures, T ≥ 65 °C, this asymptotic value is reached at t ≤ 50 min and low X_{FA} values, between 12% and 19.5% (Fig. 2b), which indicates that the Pd/AC catalyst suffers deactivation. Meanwhile, at T ≤ 55 °C, the asymptotic value is not clearly achieved during the 4 h of reaction, because the deactivation occurs more slowly, which agrees with the also slow FA decomposition rate (the X_{FA} values achieved are between 7% and 12%). Regarding the gas flow rate produced (Fig. 2c), flow rates up to 55 mL min⁻¹ can be reached at 85 °C while far lower values, of 5 mL min⁻¹, were measured at 25 °C. These

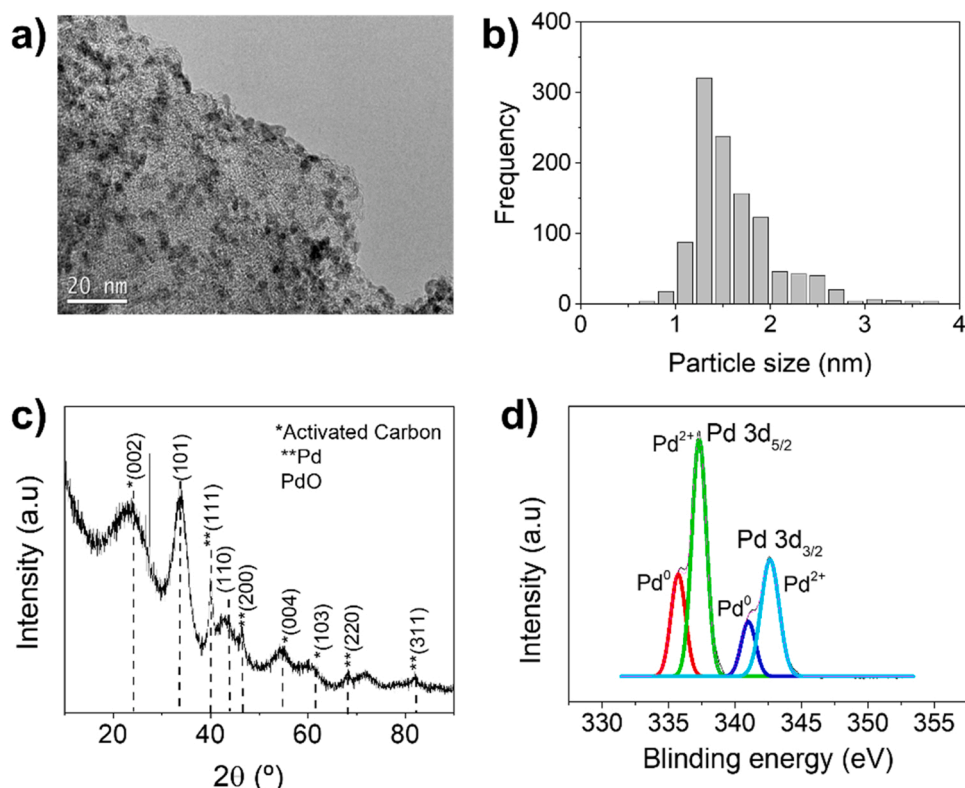


Fig. 1. Characterization results of the fresh Pd/AC catalyst: (a) TEM image, (b) Pd particle size.

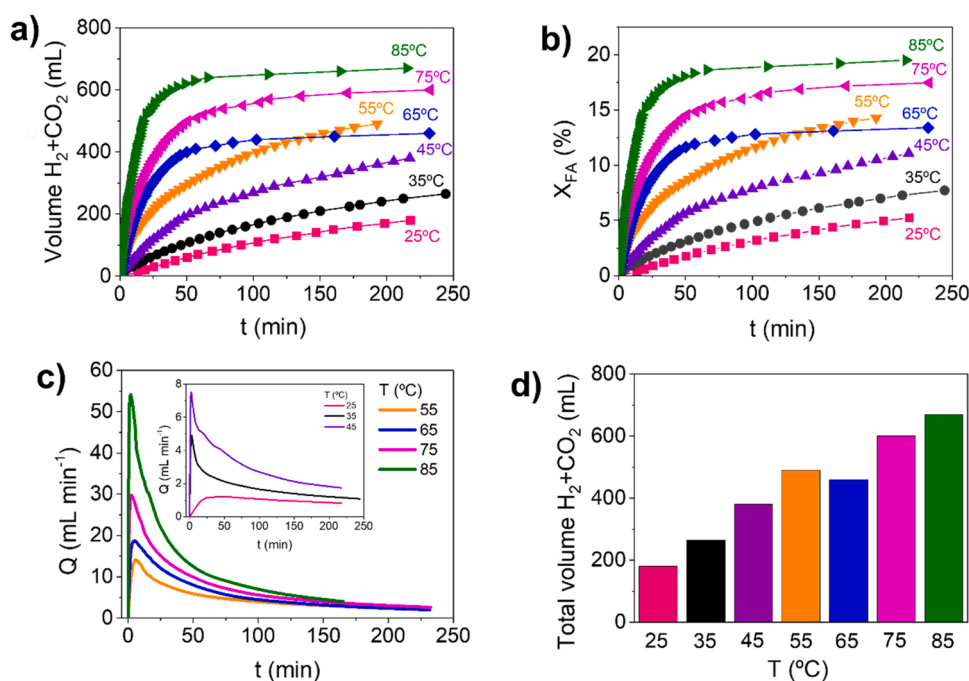


Fig. 2. Influence of the reaction temperature on the FA dehydrogenation reaction: (a) temporal evolution of the evolved gas; (b) temporal FA conversion profiles; (c) gas flow rate produced upon reaction time and (d) total volume produced upon 4 h of reaction time. Operating conditions: $C_{FA,0} = 1 \text{ M}$, $C_{CAT} = 1 \text{ g L}^{-1}$, $\omega = 650 \text{ rpm}$ and $P = 1 \text{ atm}$.

results indicate that an increase in the reaction temperature accelerates the FA decomposition rate at the early stages of the reaction, but also the catalyst deactivation. As a result, the total gas volume produced upon the 4 h of reaction is a trade-off between the H_2 production rate (or FA decomposition rate) and the deactivation rate. Note that the reaction, at

$T = 55^\circ\text{C}$, produces a higher gas volume than at 65°C (Fig. 2d) and the Pd/AC catalyst does not totally deactivate upon the 4 h of reaction (an asymptotic value of the evolved gas has not been reached). Thus, this temperature is considered the maximum operating temperature for the efficient H_2 production using the Pd/AC catalyst.

Regarding to the reaction products, the composition of the evolved gas was monitored in three reactions performed at 25, 55 and 85 °C by two different ways: (i) collecting the gas samples during a period in gas sampling bags or (ii) on-line GC monitoring by using He as carrier gas to ensure a constant gas flow in the GC, with the corresponding dilution of the sample. The typical chromatograms can be found in Fig. S2 of the Supporting Information. The H₂ and CO₂ were always the main compounds and CO was never detected. Without the He dilution, the H₂ molar concentration measured was around 50% and, in all cases, the H₂/CO₂ molar ratio measured was equal to 1. These results indicate that if the FA dehydration reaction occurs, this reaction would have a very low selectivity and, likely CO would be retained on the catalyst surface, which it can be the responsible for the catalyst deactivation.

Regarding to the Pd/CA activity, the TOF₀ values calculated by using Eq. (3) varied from 96 h⁻¹ at 25 °C to 4261 h⁻¹ at 85 °C, see Fig. 3. These values are significantly higher compared to others reported Pd carbon-based catalysts when SF is not used as additive, Table S1 of the Supporting Information collects the different values. However, the apparent activation energy is 56.2 kJ mol⁻¹, calculated from the slope of the Arrhenius equation (inset of Fig. 3), is indeed coincident with some previous works [22,27]. This result reveals some disparity between the Pd dispersion calculated from the Pd particle size measured by TEM in the literature and the one measured by CO chemisorption (D values), as performed here and in other few works [9,22,27,36]. The calculation from the particle size seems to lead to an overestimation of the Pd dispersion, and then to an underestimation of the apparent TOF values. In any case, the commercial Pd/AC catalyst herein used can be representative of the reported Pd-carbon based catalysts, as indicates the apparent activation energy value.

3.2.2. Effect of the initial FA concentration

The results obtained at different initial FA concentrations, C_{FA,0} = 0.25–2 M, and T = 75 °C are collected in Fig. 4 as the evolved gas upon reaction time (Fig. 4a) and the $(-r_{FA})_{w,0}$ evolution with the initial FA concentration (Fig. 4b). As can be seen in Fig. 4a, the FA concentration is beneficial for the H₂ production. The higher FA concentration, the higher gas volume is released (Fig. 4a) and then, the higher initial reaction rate is obtained (Fig. 4b). However, $(-r_{FA})_{w,0}$ shows a hyperbolic trendline with the FA concentration (Fig. 4b) which it can be interpreted in two ways: there is a change in the reaction order of the FA concentration from one to zero at C_{FA,0} ≥ 0.75 M or, most likely, the reaction products contribute to the catalyst deactivation.

3.2.3. Effect of the SF additive

SF is the most common additive for the FA decomposition reaction since it increases the initial concentration of formate anions in the media (HCOO⁻) [40], which are the major species adsorbed on the Pd sites to initiate the decomposition reaction [30,34,40]. As can be seen in Fig. 5, the gas volume produced at the appropriate SF:FA molar ratio of 0.8:1

[34] is higher than in absence of SF. The $(-r_{FA})_{w,0}$ values are increased 12 times at 25 °C (from 2.6 10⁻⁴ to 3.0 10⁻³ mol g⁻¹ min⁻¹) and 3.5 times at 55 °C (from 3.3 10⁻³ to 11.4 10⁻³ mol g⁻¹ min⁻¹). Thus, the beneficial effect of SF is greater at 25 °C. In addition, at 25 °C, the X_{FA} rises from 5.2% to 22.7% while at 55 °C, the increment is smaller (from 14.9% to 17.8%) because of the earlier catalyst deactivation. According to these results, it seems interesting to use the SF promoter to carry out the H₂ production at the ambient reaction temperature. Under these conditions, the largest gas volume in this study has been measured, around 800 mL in 6.7 h reaction time, without achieving a complete catalyst deactivation. To the best of our knowledge, these are one of the most promising results reported so far.

3.3. Catalyst deactivation

Despite of the Pd/AC deactivation observed during the progress of the reaction, the drying overnight at 60 °C was enough to restore its initial activity, at least when the catalyst is recycled at T ≤ 55 °C. Herein, the results obtained in successive cycles at T = 55 and 85 °C are analysed in detailed to shed light to the causes of the Pd/AC deactivation with the aim to further elucidate an appropriate deactivation model.

Fig. 6 displays the initial FA decomposition rates and FA conversions obtained in successive uses at both reaction temperatures. As can be seen, the Pd/AC catalyst maintains its activity during four cycles at 55 °C though in the last reaction, the X_{FA} slightly decreases (by a 15%). However, at 85 °C, the progressive deactivation is evident despite the drying between uses, and the X_{FA} drops by 60% after three cycles. In no case, Pd was leached out from the catalyst and detected in the liquid effluent.

These findings evidence that the major cause of deactivation is the fouling of Pd active sites by species of the reaction media that have been physically deposited on the catalyst surface or activated carbon pores hindering the access to them. These species are removed during the drying process (T = 60 °C overnight), as they can be water, FA, and reaction products such as H₂ and CO₂. Considering that a higher initial concentration of FA implies a faster reaction rate and also deactivation (Fig. 4), the Pd/AC deactivation by reaction products makes sense. Besides, the S_{BET} and the A_{ext} diminish somehow upon reaction, but the C and H content is not augmented (data collected in Table 1), results that confirm the presence of small molecules, such as H₂ and CO₂, on the activated carbon pores. In case of reaction at 85 °C, an additional factor to fouling must be considered to explain the progressive deactivation. Note that it was possible the partial recovery of the Pd/AC activity by subjecting the 3rd used Pd/AC catalyst to a thermal treatment at 150 °C for 16 h in air atmosphere (named as Reg. in Fig. 6b). This result indicates that the regeneration treatment has not been appropriate and/or the Pd/AC catalyst suffers from a slow irreversible deterioration upon use. The latter assumption is supported by the fact that the 4th used Pd/AC at T = 55 °C deactivates earlier though maintaining the same initial reaction rate, as can be seen in Fig. 6 and has been further demonstrated by recycling the 3rd used catalyst at 55 °C in a reaction performed at 25 °C (see results in Fig. S3 of the Supporting Information). To learn about this, the 1st and 3rd used catalysts have been deeply characterized. The results are collected in Table 1 and Figs. 7 and 8.

The most relevant aspects are the sintering of the Pd particle sizes as soon as the reaction occurs (Table 1 and Fig. 7), the decrease of the Pd²⁺ species upon reaction (Table 1 and Fig. S4 of the Supporting Information), the loss of Pd-PdO interface as active sites (Fig. S5) and the presence of CO₂ chemisorbed on Pd nanoparticles at T = 85 °C (Fig. 8). The TEM images and the particle size distribution of the used Pd/AC catalysts in Fig. 7 show an increase from 1.6 to 3.7 nm at 55 °C or to 4.8 nm at 85 °C, independently of the cycle use. Also, there is a decrease in the Pd dispersion upon use (see Table 1), more pronance at 85 °C according to the highest observed sintering. There is no correlation between the activity observed in successive cycles (Fig. 6) and the increment in the particle size, therefore, this sintering does not cause the

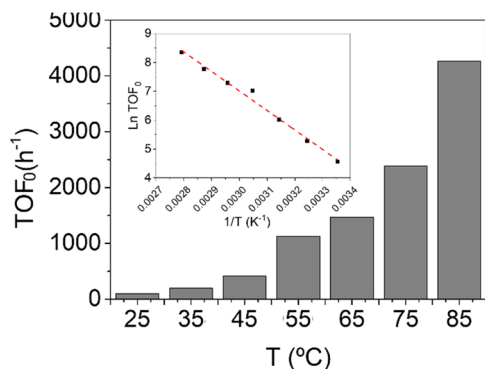


Fig. 3. TOF values at different reaction temperature. Inset: Arrhenius plot of Pd/AC.

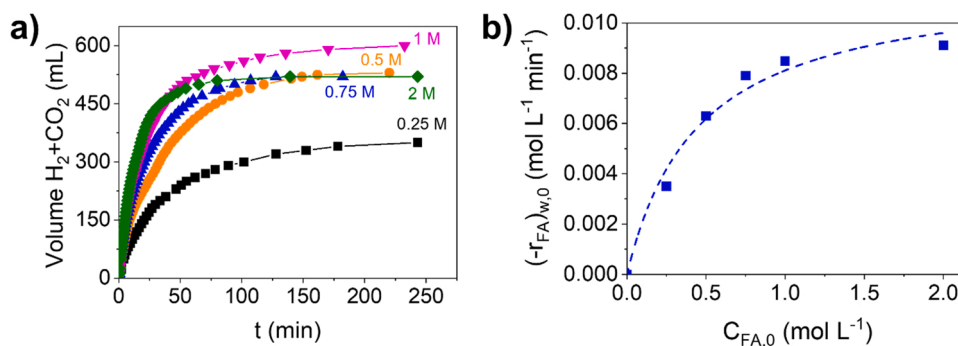


Fig. 4. Influence of the initial FA concentration on FA dehydrogenation reaction: (a) temporal evolution of the evolved gas and (b) initial reaction rates vs. initial concentration. Operating conditions: $T = 75\text{ }^{\circ}\text{C}$, $C_{CAT} = 1\text{ g L}^{-1}$, $\omega = 650\text{ rpm}$ and $P = 1\text{ atm}$.

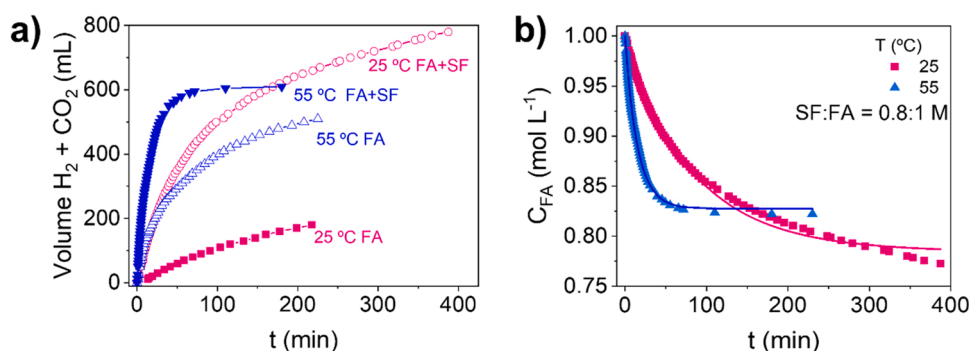


Fig. 5. Influence of the SF additive on the FA dehydrogenation reaction: (a) temporal evolution of the evolved gas and (b) temporal FA concentration profiles (experimental data in symbols and calculated by the model, Eq. (13), in lines). Operating conditions: $C_{FA,0} = 1\text{ M}$, $C_{SF,0} = 0.8\text{ M}$, $C_{CAT} = 1\text{ g L}^{-1}$, $\omega = 650\text{ rpm}$, $T = 25$ and $55\text{ }^{\circ}\text{C}$ and $P = 1\text{ atm}$.

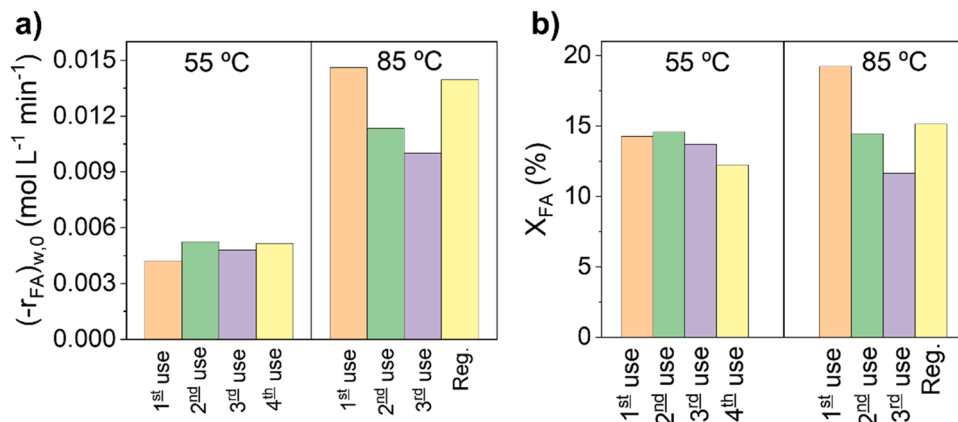


Fig. 6. Initial FA decomposition rates (a) and FA conversions (b) obtained in successive uses at different reaction temperatures. Operating conditions: $C_{FA,0} = 1\text{ M}$, $C_{CAT} = 1\text{ g L}^{-1}$, $T = 55$ and $85\text{ }^{\circ}\text{C}$, $\omega = 650\text{ rpm}$ and $P = 1\text{ atm}$.

Pd/AC catalyst deactivation.

On the other hand, the Pd²⁺/Pd⁰ atomic ratio reduces from 2.4 in the fresh to 0.88 and 0.79 after 3rd use at $T = 55\text{ }^{\circ}\text{C}$ and $T = 85\text{ }^{\circ}\text{C}$, respectively, see the data in Table 1 and XPS spectra in Fig. S4. The decline in the Pd²⁺ species is consequence of the Pd nanoparticles sintering and, also, of its reduction by the hydrogen produced upon reaction [22,31,34]. These results are supporting by the XRD spectra of the 3rd used Pd/AC catalysts, provided in Fig. S5 of the Supporting Information, because the peaks assigned to the crystalline PdO phases were not detected. After the regeneration of the catalyst employed at $T = 85\text{ }^{\circ}\text{C}$, the Pd²⁺/Pd⁰ atomic ratio is not recovered (Pd²⁺/Pd⁰ = 0.70 at.), neither the crystalline PdO phases (data do not shown), while the

catalyst activity partially does (Fig. 6). The fact that the used and regenerated catalysts recover most of the activity though they suffer from quicker deactivation (as shown in Figs. S3 and 6) could be related to the loss of the Pd-PdO interface. In principle, the PdO could help to the release the hydrogen, or any other species present on the Pd⁰ active sites [30]. Further studies would be needed to precisely determine the contribution of the crystalline PdO phase.

Finally, the presence of CO₂ irreversibly adsorbed (or chemisorbed) on Pd nanoparticles has been detected by ATR only in the Pd/AC catalyst used at $85\text{ }^{\circ}\text{C}$ and further dried at $60\text{ }^{\circ}\text{C}$ overnight, peaks at 2250–2750 cm⁻¹ [41–43]. The CO₂ poisoning can be responsible of the progressive loss of activity upon successive cycles at $T = 85\text{ }^{\circ}\text{C}$ since the

Table 1

Pd dispersion (D) and Pd particle size (d_{Pd}), atomic surface ratio Pd^{2+}/Pd^0 , S_{BET} , A_{ext} and bulk C and H content of different Pd/AC catalysts.

Pd/AC catalyst*	D (%)	d_{Pd} (nm)	Pd^{2+}/Pd^0 (at.)	S_{BET} ($m^2 g^{-1}$)	A_{ext} ($m^2 g^{-1}$)	C (wt %)	H (wt %)
Fresh	24	1.6	2.4	887	404	77.7	1.40
1st use	19	3.8	n.m.	835	380	78.3	0.92
T = 55 °C							
3rd use	17	3.6	0.88	843	387	78.1	1.01
T = 55 °C							
1st use	16.5	4.6	n.m.	812	356	79.3	1.15
T = 85 °C							
3rd use	14.0	4.9	0.79	857	381	78.0	1.45
T = 85 °C							

*The catalysts were dried at 60 °C overnight before the analysis **n.m. not measured.

CO₂ chemisorbed on the Pd sites is still present in the dried catalyst and even in the regenerated catalyst (see Fig. 8a). Remarkable, chemisorbed CO on Pd nanoparticles was never detected. No bands were obtained in the region 1975–2252 cm⁻¹ in the ATR spectra of any of the used catalysts [41,44], which confirms that the FA decomposition upon the Pd/AC catalyst occurs by the dehydrogenation reaction solely producing H₂ and CO₂. Palladium hydride was also not produced upon reaction. No peaks were observed at 2150 cm⁻¹ in the ATR spectra [44] and the peaks in the XRD spectra corresponding to metallic Pd in the used Pd/AC catalysts have not been shifted with respect to those of the fresh catalyst [45,46]. Finally, bands ascribed to the interaction between FA and Pd nanoparticles, typically 1720–1739 cm⁻¹ for CO, 2938 cm⁻¹ for CH and 1578 cm⁻¹ for OCO vibrations from FA molecules [36,47] cannot be exclusively identified in the used catalysts since these bands are also present in the fresh Pd/AC catalyst, due to the presence of those groups in the activated carbon support. However, these spectral bands are not more intense than in the fresh catalyst, therefore, the presence of FA

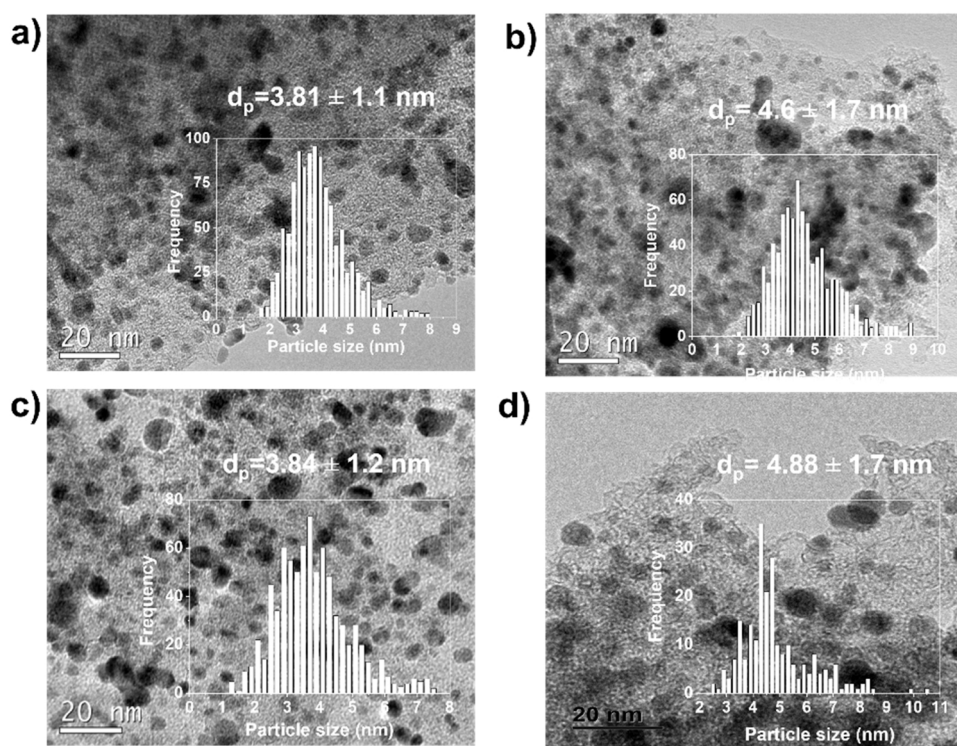


Fig. 7. TEM images and Pd particle size distribution of the used catalysts: (a) 1st use at T = 55 °C, (b) 1st use at T = 85 °C, (c) 3rd use at T = 55 °C and (d) 3rd use at T = 85 °C.

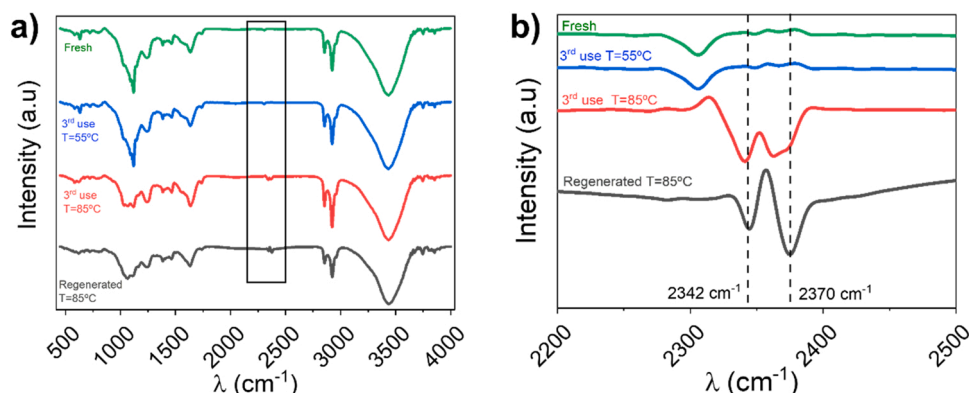


Fig. 8. (a) ATR-IR spectra and (b) zoom in the window from 2200 to 2500 cm⁻¹ of the fresh, used and regenerated catalysts in the slurry reactor.

poisoning the Pd active sites can be also excluded. In conclusion, the above results demonstrate that the CO₂ produced upon the FA decomposition is the main responsible for the Pd/AC deactivation due to its chemisorption on Pd active sites.

To find more evidence about this unprecedented result, an additional FA decomposition experiment was carried out after pretreatment of the fresh Pd/AC catalyst with CO₂. However, the adsorption of CO₂ occurred on the activated carbon support instead on the Pd sites, as deduced from the characterization of the CO₂-treated Pd/AC catalyst by ATR spectroscopy and TGA-MS (see Fig. S6a-d of the Supporting Information). On the other hand, the CO₂-treated Pd/AC catalyst exhibited a slightly higher activity than its counterpart (Fig. S6e) which it may be caused by the enhanced acidity of the CO₂-treated Pd/AC catalyst [28]. The pH_{slurry} of the Pd/AC catalyst diminishes from 5.5 to 4.5 after the CO₂ treatment.

These results show that the adsorption of CO₂ molecules from a gas stream on Pd nanoparticles is a completely different scenario as the one taking place during the reaction. In the latter, CO₂ is produced on the Pd surface, and the CO₂ adsorbed species remain on the Pd sites, causing the poisoning when high reaction temperatures (above 55 °C) are used. At high temperatures, the FA decomposition rate, or the production of CO₂, is faster and therefore, higher amounts of CO₂ molecules are simultaneously present on the Pd sites. The CO₂ accumulated on the Pd sites can be better detected by infrared spectroscopy and this accumulation can compensate the easy desorption of the CO₂ molecules because of the low molecular bonding strength with the Pd sites at high temperatures. Therefore, at high temperature, there is a greater probability that the CO₂ molecules can occupy the Pd sites. The temperature threshold for this phenomenon in batch mode is between 60 and 65 °C (see Fig. S7 of the Supporting Information).

3.4. Kinetic modeling: parameter estimation

The FA dehydrogenation rate was first modeled considering the experimental concentration vs. *t* data at different reaction temperatures (Fig. 2d). Different kinetic models, viz. potential equations, LHHW and ER kinetics, have been considered to fit the initial data before the

deactivation. The best-fit kinetic rate equation found was a first-order equation with an activation energy value of 56.2 kJ mol⁻¹, Fig. 9a. Next, the activity was calculated at each temperature and C_{FA,0} = 1 M, see Fig. 9b, by Eq. (5), where the numerical values of the FA decomposition rates are obtained as the derivative of FA concentration versus time (Fig. 9c) using OriginLab 2017. As can be seen in Fig. 9b, the activity decreases exponentially with the reaction time. Therefore, the activity decay is also described by a first-order power law equation (m=1 in Eq. (6)). The lines in Fig. 9b show the calculated activity values. The estimated *k_d* values increase with the temperature at a given initial FA concentration (C_{FA,0} = 1 M) and follows the Arrhenius equation, with an activation energy equal to 41.7 kJ mol⁻¹. This is in accordance with a deactivation caused by the poisoning of CO₂ which is faster produced at higher temperatures.

According to the above results, the FA dehydrogenation reaction rate can be expressed as:

$$(-r_{FA})_w = k_{FA} \cdot C_{FA} \cdot \exp(-k_d \cdot t) \quad (7)$$

and the corresponding integrated equation is:

$$C_{FA} \left(\frac{\text{mol}}{\text{L}} \right) = C_{FA,0} + \exp \left[\left(\frac{k_{FA}}{k_d} \right) \cdot (\exp(-k_d \cdot t) - 1) \right] \quad (8)$$

Regarding to the effect of the initial FA concentration on the dehydrogenation reaction, the hyperbolic trend observed between the initial reaction rate and initial FA concentration at T = 75 °C in Fig. 4b can only be explained if this variable is related to the catalyst deactivation since for first-order equations, a linear trend should be obtained and also, the same temporal X_{FA} profile whatever the initial FA concentration used (which is not the case, see Fig. S8a of the Supporting Information). To demonstrate this, *k_d* values were estimated by fitting Eq. (8) to the experimental FA concentration vs. *t* curves at different initial FA concentration and fixing *k_{FA}* = 0.008 min⁻¹ as corresponds to T = 75 °C. The estimated *k_d* values shows a linear relationship with the initial FA concentration (Fig. S8b of the Supporting Information) meaning that the higher initial FA concentration, the faster deactivation, as expected by the faster production of CO₂. According to this, the $(-r_{FA})_w$ and C_{FA} can

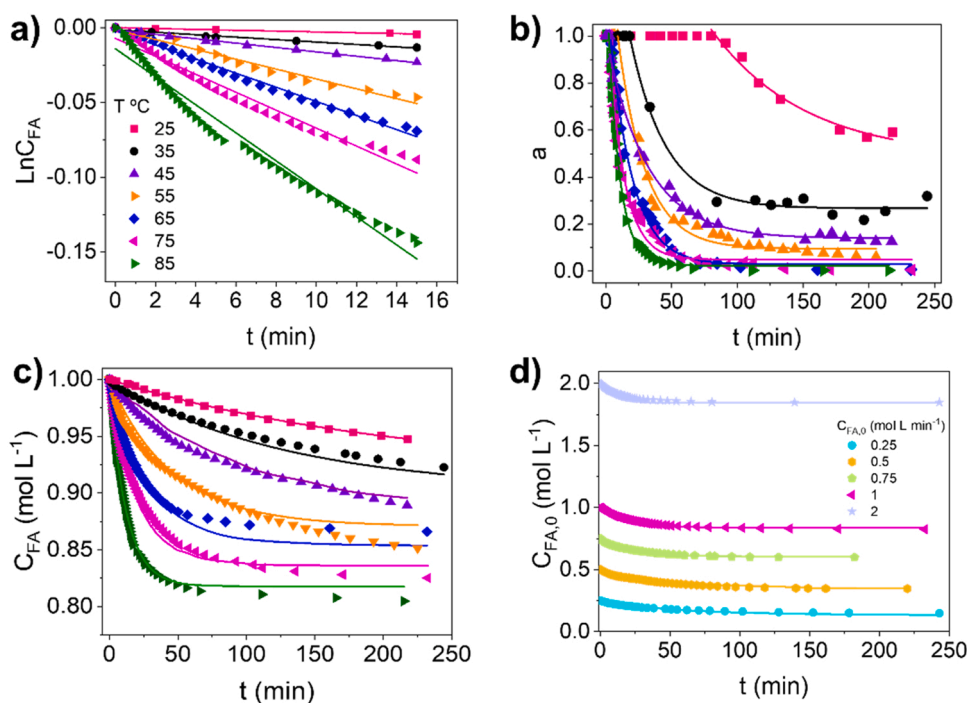


Fig. 9. (a) FA concentration vs. time at the beginning of the reaction at C_{FA,0} = 1 M, (b) activity vs. time at C_{FA,0} = 1 M, (c) FA concentration vs. time considering the deactivation at C_{FA,0} = 1 M and (d) at T = 75 °C. In c) and d) the symbols are the experimental data and curves the predicted ones by Eq. (12).

be expressed as:

$$(-r_{FA})_w = k_{FA} \cdot C_{FA} \cdot \exp(-k_1 \cdot C_{FA,0} \cdot t) \quad (9)$$

$$C_{FA} \left(\frac{\text{mol}}{\text{L}} \right) = C_{FA,0} + \exp \left[\left(\frac{k_{FA}}{k_1 \cdot C_{FA,0}} \right) \cdot (\exp(-k_1 \cdot C_{FA,0} \cdot t) - 1) \right] \quad (10)$$

where $k_1 = 0.008 \text{ L mol}^{-1} \text{ min}^{-1}$ at $T = 75^\circ \text{C}$.

The fitting of Eq. (10) to the experimental FA concentration profiles at different operating conditions in absence of the SF additive results in the following expression to describe the FA concentration:

$$C_{FA} \left(\frac{\text{mol}}{\text{L}} \right) = C_{FA,0} \cdot \exp \left[\left(\frac{(9.87 \pm 3.95) \cdot 10^5 \cdot \exp\left(-\frac{53.6 \pm 11.6}{R \cdot T}\right)}{(2.54 \pm 1.48) \cdot 10^5 \cdot \exp\left(-\frac{44.3 \pm 16.0}{R \cdot T}\right) \cdot C_{FA,0}} \right) \cdot \left(\exp\left(- (2.54 \pm 1.48) \cdot 10^5 \cdot \exp\left(-\frac{44.3 \pm 16.0}{R \cdot T}\right) \cdot C_{FA,0} \cdot t\right) - 1 \right) \right] \quad (11)$$

in which the kinetic rate constants, $k_{FA} (\text{min}^{-1})$ and $k_1 (\text{L mol}^{-1} \text{ min}^{-1})$ have been substituted by the Arrhenius equation. The activation energies are provided in kJ mol^{-1} . From this Eq. (11), it is possible to quantify, by stoichiometry of the reaction, the concentration of the H_2 and CO_2 products.

The good agreement found between the experimental and calculated concentration values are shown in Figures 9c-d and the parity plot in Fig. S9a-b of the Supporting Information. Also, by Eq. (11), the performance at reaction temperatures of 50 and 60°C is adequately predicted (Fig. S10). These data have not been used to carry out the kinetic modeling, but they contribute to validate it. Thus, the following kinetic model equation for the FA dehydrogenation reaction over Pd/AC catalysts for CO-free hydrogen production is elucidated:

$$(-r_{FA})_w \left(\frac{\text{mol}_{FA}}{\text{g}_{CAT} \cdot \text{min}} \right) = 9.87 \cdot 10^5 \cdot \exp\left(-\frac{53.6 \text{ kJ mol}^{-1}}{R \cdot T}\right) \cdot C_{FA} \cdot \exp\left(-2.54 \cdot 10^5 \cdot \exp\left(-\frac{44.3 \text{ kJ mol}^{-1}}{R \cdot T}\right) \cdot C_{FA,0} - t\right) \quad (12)$$

when SF is used as additive to promote the reaction, the same kinetic model is valid, but the estimated values of the kinetic parameters are different:

$$(-r_{FA})_w \left(\frac{\text{mol}_{FA}}{\text{g}_{CAT} \cdot \text{min}} \right) = (2.70 \pm 0.6) 10^4 \cdot \exp\left(-\frac{(39.9 \pm 0.6) \text{ kJ mol}^{-1}}{R \cdot T}\right) \cdot C_{FA} \cdot \exp\left(- (1.67 \pm 0.5) \cdot 10^6 \cdot \exp\left(-\frac{(46.6 \pm 0.7) \text{ kJ mol}^{-1}}{R \cdot T}\right) \cdot C_{FA,0} - t\right) \quad (13)$$

The value of the activation energy for FA decomposition, 39.9 kJ mol^{-1} , is similar as those reported in literature when SF is used, see Table S1 [26,29,35,37,39]. The good fitness between the FA concentration calculated from Eq. (13) and the experimental data can be seen in Fig. 5b and the parity plot provided in Fig. S9c of the Supporting Information.

The elucidated models for the FA decomposition to produce H_2 , in

absence and presence of SF additive, Eqs. (12) and (13), respectively, demonstrate that two operational variables ruled out the Pd/AC deactivation, the FA concentration fed to the reactor and the reaction temperature. The higher the values of these variables, the faster the chemical reaction rate and, also, the deactivation since it implies a most rapid production of CO_2 , the main product responsible for the deactivation. At reaction temperatures above 55°C , the Pd/AC deactivation becomes irreversible since the CO_2 is chemisorbed on the Pd active sites. Besides, the use of SF as promoter enhances the FA decomposition rate and, to a lesser extent, also the deactivation rate. Thus, the most favorable condition for the Pd/AC catalyst durability is to perform the

FA decomposition reaction at room temperature with SF as additive.

The kinetic model here elucidated will allow the further simulation of the process in different catalytic reactors under several operating conditions to select the reactor type and the reactor well-suited design with its appropriate operation mode to prevent or slow catalyst deactivation.

4. Conclusions

An original kinetic model for FA dehydrogenation on Pd/AC catalysts in liquid phase that quantifies the formation of H_2 and CO_2 products and considers catalyst deactivation has been established. The kinetic equation corresponds to a first order reaction for FA concentration and for the catalyst activity and it is valid in a wide range of

operating conditions. The activation energy for FA dehydrogenation is 53.6 kJ mol^{-1} and for the deactivation is 44.3 kJ mol^{-1} . In presence of SF as additive, the activation energy for the reaction diminishes to 40 kJ mol^{-1} . The deactivation rate constant depends on the reaction temperature and initial FA concentration fed to the reactor. The recovery of the initial activity can be achieved by drying the catalyst at 60°C , to remove the species of the reaction media that foul the Pd active sites, though there is a progressive and irreversible catalyst deactivation. The main species responsible for the Pd/AC deactivation is the CO_2 product that remains chemisorbed on Pd active sites at reaction temperatures above 55°C , when the FA conversion is significant and also the production of CO_2 initially adsorbed on the Pd sites. Also, the loss of the Pd^{2+} species, in particular, the crystalline PdO phase can contribute to a quicker catalyst deactivation. The sintering of the Pd nanoparticles do not significantly affect to the catalyst activity, at least at reaction temperatures as high as 85°C .

This kinetic study will further allow the selection of the most suitable reactor technology and the optimization of the process conditions to moves towards the scaling-up of a commercial technology to extract hydrogen on demand.

CRediT authorship contribution statement

Celia Martin: Investigation, Writing – original draft, Software, Data curation. **Asuncion Quintanilla:** Conceptualization, Methodology, Resources, Writing – review & editing, Visualization. **Gonzalo Vega:** Investigation, Validation, Formal analysis. **Jose A. Casas:** Supervision, Project administration, Funding acquisition.

Declaration of Competing Interest

The authors declare the following financial interests/personal relationships which may be considered as potential competing interests: Jose A. Casas reports financial support was provided by Government of Spain. Jose A. Casas reports financial support was provided by Community of Madrid.

Data Availability

Data will be made available on request.

Acknowledgments

The authors thank the financial support by the Community of Madrid through the project S2018/EMT-4341 and the Government of Spain through the project PID2019-105079RB-I00 (MCIU/AEI/FEDER, UE). Also, C. Martin acknowledges the Community of Madrid and the European Social Fund for the financing received through the contract PEJ-2020-AI/AMB18976. G. Vega acknowledges the Universidad Autónoma de Madrid for the Predoctoral contract. The authors thank Juliana Mejía for her permanent technical assistance, the "Servicio Interdepartamental de Investigación" (Sidi) of the Universidad Autonoma de Madrid (UAM), and in particular Luis Larumbe from FTIR lab and Josué Friedrich from TXRF lab, the "Centro Nacional de Microscopía Electrónica" (ICTS-CNME) of the Universidad Complutense de Madrid (UCM), in particular to Esteban Urones and the "Servicios Centrales de Apoyo a la Investigación" (SCAI), in particular to Maria del Valle Martínez de Yuso and María Dolores Marqués from Sólidos Porosos Lab.

Appendix A. Supplementary material

Supplementary data associated with this article can be found in the online version at [doi:10.1016/j.apcatb.2022.121802](https://doi.org/10.1016/j.apcatb.2022.121802).

References

- [1] E. Papadakis, G. Tsatsaronis, Challenges in the decarbonization of the energy sector, *Energy* 205 (2020), 118025, <https://doi.org/10.1016/j.energy.2020.118025>.
- [2] H.T. Hwang, A. Varma, Hydrogen storage for fuel cell vehicles, 43–38, *Curr. Opin. Chem. Eng.* 5 (2014), <https://doi.org/10.1016/j.coche.2014.04.004>.
- [3] E. Rivard, M. Trudeau, K. Zaghib, Hydrogen storage for mobility: a review, *Materials* 12 (2019) 1973, <https://doi.org/10.3390/ma12121973>.
- [4] L.J. Murray, M. Dincă, J.R. Long, Hydrogen storage in metal-organic frameworks, *Chem. Soc. Rev.* 38 (2009) 1294–1314, <https://doi.org/10.1039/B802256A>.
- [5] F. Schüth, B. Bogdanović, M. Felderhoff, Light metal hydrides and complex hydrides for hydrogen storage, *Chem. Commun.* 20 (2004) 2249–2258, <https://doi.org/10.1039/B406522K>.
- [6] C. Lang, Y. Jia, J. Liu, H. Wang, L. Ouyang, M. Zhu, X. Yao, Dehydrogenation and reaction pathway of perovskite-type $\text{NH}_4\text{Ca}(\text{BH}_4)_3$, *Prog. Nat. Sci. Mater. Int.* 28 (2018) 194–199, <https://doi.org/10.1016/j.pnsc.2018.02.002>.
- [7] M. Yadav, Q. Xu, Liquid-phase chemical hydrogen storage materials, *Energy Environ. Sci.* 5 (2012) 9698–9725, <https://doi.org/10.1039/C2EE22937D>.
- [8] C. Lang, Y. Jia, X. Yao, Recent advances in liquid-phase chemical hydrogen storage, *Energy Storage Mater.* 26 (2020) 290–312, <https://doi.org/10.1016/j.ensm.2020.01.010>.
- [9] F. Sánchez, D. Motta, A. Roldan, C. Hammond, A. Villa, N. Dimitratos, Hydrogen generation from additive-free formic acid decomposition under mild conditions by Pd/C: experimental and DFT studies, *Top. Catal.* 61 (2018) 254–266, <https://doi.org/10.1007/s11244-018-0894-5>.
- [10] T. Semelsberger, J. Graetz, A. Sutton, E.C. Rönnebro, Engineering challenges of solution and slurry-phase chemical hydrogen storage materials for automotive fuel cell applications, *Molecules* 26 (2021) 1722, <https://doi.org/10.3390/molecules26061722>.
- [11] U. Eberle, M. Felderhoff, F. Schueth, Chemical and physical solutions for hydrogen storage, *Angew. Chem. Int. Ed.* 48 (2009) 6608–6630, <https://doi.org/10.1002/anie.200806293>.
- [12] Z. Abidin, C. Tang, Y. Liu, K. Catchpole, Large-scale stationary hydrogen storage via liquid organic hydrogen carriers, *iScience* 24 (2021), 102966, <https://doi.org/10.1016/j.isci.2021.102966>.
- [13] J. Zheng, H. Zhou, C.G. Wnag, E. Ye, J.W. Xu, X.J. Loh, Z. Li, Current research progress and perspectives on liquid hydrogen rich molecules in sustainable hydrogen storage, *Energy Storage Mater.* 35 (2021) 695–722, <https://doi.org/10.1016/j.ensm.2020.12.007>.
- [14] P.C. Rao, M. Yoon, Potential liquid-organic hydrogen carrier (LOHC) systems: a review on recent progress, *Energies* 13 (2020) 6040, <https://doi.org/10.3390/en13226040>.
- [15] E. Gianotti, M. Taillades-Jacquín, J. Rozière, D.J. Jones, High purity hydrogen generation via dehydrogenation of organics carriers: a review on the catalytic process, *ACS Catal.* 8 (2018) 4660–4680, <https://pubs.acs.org/doi/10.1021/acscatal.7b04278>.
- [16] J.Y. Cho, H. Kim, J.E. Oh, B.Y. Park, Recent advances in homogeneous/heterogeneous catalytic hydrogenation and dehydrogenation for potential liquid organic hydrogen carrier (LOHC) systems, *Catalysts* 11 (2021) 1497, <https://doi.org/10.3390/catal11121497>.
- [17] A.K. Singh, S. Singh, A. Kumar, Hydrogen energy future with formic acid: a renewable chemical hydrogen storage system, *Catal. Sci. Technol.* 6 (2016) 12–40, <https://doi.org/10.1039/C5CY01276G>.
- [18] L. Zhang, W. Wu, Z. Jiang, T. Fang, A review on liquid-phase heterogeneous dehydrogenation of formic acid: recent advances and perspectives, *Chem. Pap.* 72 (2018) 2121–2135, <https://doi.org/10.1007/s11696-018-0469-8>.
- [19] H. Zhong, M. Iguchi, M. Chatterjee, Y. Himeda, Q. Xu, H. Kawanami, Formic acid-based liquid organic hydrogen carrier system with heterogeneous catalysts, *Adv. Sustain. Syst.* 2 (2018) 1700161, <https://doi.org/10.1002/advs.201700161>.
- [20] F. Valentini, V. Kozell, C. Petrucci, A. Marrocchi, Y. Gu, D. Gelman, L. Vaccaro, Formic acid, a biomass-derived source of energy and hydrogen for biomass upgrading, *Energy Environ. Sci.* 12 (2019) 2646–2664, <https://doi.org/10.1039/C9EE01747J>.
- [21] P. Preuster, J. Albert, Biogenic formic acid as a green hydrogen carrier, *Energy Technol.* 6 (2018) 501–509, <https://doi.org/10.1002/ente.201700572>.
- [22] C. Hu, J.K. Pulleri, S.W. Ting, K.Y. Chan, Activity of Pd/C for hydrogen generation in aqueous formic acid solution, *Int. J. Hydrog. Energy* 39 (2014) 381–390, <https://doi.org/10.1016/j.ijhydene.2013.10.067>.
- [23] X. Wang, Q. Meng, L. Gao, Z. Jin, J. Ge, C. Liu, W. Xing, Recent progress in hydrogen production from formic acid decomposition, *Int. J. Hydrog. Energy* 43 (2018) 7055–7071, <https://doi.org/10.1016/j.ijhydene.2018.02.146>.
- [24] R. Xu, W. Lu, S. Toan, Z. Zhou, C.K. Russell, Z. Sun, Thermocatalytic formic acid dehydrogenation: recent advances and emerging trends, *J. Mater. Chem. A* 9 (2021) 24241–24260, <https://doi.org/10.1039/D1TA05910F>.
- [25] M. Naviani-García, K. Mori, D. Salinas-Torres, Y. Kuwahara, H. Yamashita, New approaches toward the hydrogen production from formic acid dehydrogenation over Pd-based heterogeneous catalysts, *Front. Mater.* 6 (2019) 44, <https://doi.org/10.3389/fmats.2019.00044>.
- [26] J. Li, W. Chen, H. Zhao, X. Zheng, L. Wu, H. Pan, J. Lu, Y. Chen, J. Lu, Size-dependent catalytic activity over carbon-supported palladium nanoparticles in dehydrogenation of formic acid, *J. Catal.* 352 (2017) 371–381, <https://doi.org/10.1016/j.jcat.2017.06.007>.
- [27] Y. Kim, D.H. Kim, Understanding the effect of Pd size on formic acid dehydrogenation via size-controlled Pd/C catalyst prepared by NaBH_4 treatment, *Appl. Catal. B Environ.* 244 (2019) 684–693, <https://doi.org/10.1016/j.apcatb.2018.12.008>.
- [28] H.J. Jeon, Y.M. Chung, Hydrogen production from formic acid dehydrogenation over Pd/C catalyst: effect of metal and support properties on the catalytic performance, *Appl. Catal. B Environ.* 210 (2017) 212–222, <https://doi.org/10.1016/j.apcatb.2017.03.070>.
- [29] M. Yao, W. Liang, H. Chen, X. Zhang, Efficient hydrogen production from formic acid using nitrogen-doped activated carbon supported Pd, *Catal. Lett.* 150 (2020) 2377–2384, <https://doi.org/10.1007/s10562-020-03141-y>.
- [30] Q. Lv, Q. Meng, W. Liu, N. Sun, K. Jiang, L. Ma, Z. Peng, W. Cai, C. Liu, J. Ge, L. Liu, W. Xing, Pd-PdO interface as active site for HCOOH selective dehydrogenation at ambient conditions, *J. Phys. Chem. C* 122 (2018) 2081–2088, <https://doi.org/10.1021/acs.jpcc.7b08105>.
- [31] M. Cai, D. Padovan, C. Hammond, Continuous production of hydrogen from formic acid decomposition over heterogeneous nanoparticle catalysts: from batch to continuous flow, *ACS Catal.* 9 (2019) 9188–9198, <https://pubs.acs.org/doi/10.1021/acscatal.9b01977>.
- [32] K. Tedsree, T. Li, S. Jones, C.W.A. Chan, K.M.K. Yu, P.A. Bagot, E.A. Marquis, G.D. W. Smith, S.C.E. Tsang, Hydrogen production from formic acid decomposition at room temperature using a Ag-Pd core-shell nanocatalyst, *Nat. Nanotechnol.* 6 (2011) 302–307, <https://doi.org/10.1038/nnano.2011.42>.
- [33] Y. Ge, X. Qin, A. Li, Y. Deng, L. Lin, M. Zhang, Q. Yu, S. Li, M. Peng, Y. Xu, X. Zhao, M. Xu, W. Zhou, S. Yao, D. Ma, Maximizing the synergistic effect of CoNi catalyst on α -MoC for robust hydrogen production, *J. Am. Chem. Soc.* 143 (2020) 628–633, <https://pubs.acs.org/doi/10.1021/jacs.0c11285>.
- [34] Y. Kim, S.H. Kim, H.C. Ham, D.H. Kim, Mechanistic insights on aqueous formic acid dehydrogenation over Pd/C catalyst for efficient hydrogen production, *J. Catal.* 389 (2020) 506–516, <https://doi.org/10.1016/j.jcat.2020.06.033>.
- [35] Q.L. Zhu, N. Tsumori, Q. Xu, Immobilizing extremely catalytically active palladium nanoparticles to carbon nanospheres: a weakly-capping growth approach, *J. Am.*

- Chem. Soc. 137 (2015) 11743–11748, <https://pubs.acs.org/doi/abs/10.1021/jacs.5b06707>.
- [36] L. Jia, D.A. Bulushev, J.R.L. Ross, Formic acid decomposition over palladium based catalysts doped by potassium carbonate, *Catal. Today* 259 (2016) 453–459, <https://doi.org/10.1016/j.cattod.2015.04.008>.
- [37] L. Di, J. Zhang, M. Craven, Y. Wang, H. Wang, X. Zhang, X. Tu, Dehydrogenation of formic acid over Pd/C catalysts: insight into the cold plasma treatment, *Catal. Sci. Technol.* 10 (2020) 6129–6138, <https://doi.org/10.1039/D0CY00055H>.
- [38] H. Gao, R. Ma, X. Wang, Z. Jin, S. Hou, W. Xu, Q. Meng, J. Ge, C. Liu, W. Xing, Activating the Pd-based catalysts via tailoring reaction interface towards formic acid dehydrogenation, 17575–1758, *Int. J. Hydrog. Energy* 45 (35) (2020), <https://doi.org/10.1016/j.ijhydene.2020.04.289>.
- [39] H. Wang, Y. Zhou, Q. Zhao, X. Zhang, L. Di, NH₃ plasma synthesis of N-doped activated carbon supported Pd catalysts with high catalytic activity and stability for HCOOH dehydrogenation, *Int. J. Hydrog. Energy* 45 (41) (2020) 21380–21391, <https://doi.org/10.1016/j.ijhydene.2020.05.209>.
- [40] X. Wang, G. Qia, C. Tan, Y. Lia, J. Guoa, X. Pang, S. Zhang, Pd/C nanocatalyst with high turnover frequency for hydrogen generation from the formic acid–formate mixtures, *J. Hydrog. Energy* 39 (2) (2014) 837–843, <https://doi.org/10.1016/j.ijhydene.2013.10.154>.
- [41] J. Wang, H. Zhang, H. Jiang, W. Cai, From HCOOH to CO at Pd electrodes: a surface-enhanced infrared spectroscopy study, *J. Am. Chem. Soc.* 133 (38) (2011) 14876–14879, <https://doi.org/10.1021/ja205747j>.
- [42] P. Xu, F.D. Bernal-Juan, L. Lefferts, Effect of oxygen on formic acid decomposition over Pd catalyst, *J. Catal.* 304 (2021) 342–352, <https://doi.org/10.1016/j.jcat.2020.10.032>.
- [43] A. Kosider, D. Blaumeiser, S. Schötz, P. Preuster, A. Bösmann, P. Wasserscheid, J. Libuda, T. Bauer, Enhancing the feasibility of Pd/C-catalyzed formic acid decomposition for hydrogen generation – catalyst pretreatment, deactivation, and regeneration, *Catal. Sci. Technol.* 11 (2021) 4259–4271, <https://doi.org/10.1039/D1CY00300C>.
- [44] L.J. Hoyos, M. Primet, H. Praliaud, Sulfur poisoning and regeneration of palladium based catalysts: Part II: influence of adsorbed sulfur on the deactivation by carbonaceous deposits, *J. Chem. Soc. Faraday Trans.* 88 (22) (1992) 3367–3373.
- [45] S.F. Parker, H.C. Walker, S.K. Callear, E. Grunewald, T. Petzold, D. Wolf, K. Mobus, J. Adam, S.D. Wieland, M. Jiménez-Ruiz, P.W. Albers, The effect of particle size, morphology and support on the formation of palladium hydride in commercial catalysts, *Chem. Sci.* 10 (2019) 480, <https://doi.org/10.1039/c8sc03766c>.
- [46] Z. Zhao, X. Huang, M. Li, G. Wang, C. Lee, E. Zhu, X. Duan, Y. Huang, Synthesis of stable shape-controlled catalytically active β -palladium hydride, *J. Am. Chem. Soc.* 137 (2015) 15672–15675, <https://doi.org/10.1021/jacs.5b11543>.
- [47] G.C. Cabilla, A.L. Bonivardi, M.A. Baltanás, Infrared study of the adsorption of formic acid on clean and Ca-promoted Pd/SiO₂ catalysts, *Appl. Catal. A Gen.* 255 (2) (2003) 181–195, [https://doi.org/10.1016/S0926-860X\(03\)00546-5](https://doi.org/10.1016/S0926-860X(03)00546-5).